



Article

Investigation of Wall Effect on Packing Structures and Purge Gas Flow Characteristics in Pebble Beds for Fusion Blanket by Combining Discrete Element Method and Computational Fluid Dynamics Simulation

Baoping Gong ^{1,*}, Hao Cheng ¹, Bing Zhou ¹, Juemin Yan ¹, Long Wang ¹, Long Zhang ¹, Yongjin Feng ² and Xiaoyu Wang ¹

¹ Southwestern Institute of Physics, Chengdu 610041, China

² Nuclear Power Institute of China, Chengdu 610041, China

* Correspondence: gongbp@swip.ac.cn; Tel.: +86-183-8200-1656

Abstract: In a tritium-breeding blanket of a fusion reaction, helium, used as a tritium-purging gas, will purge the tritium breeder pebble beds to extract the tritium in blanket. The purge gas flow characteristics will affect the tritium extraction efficiency. The effect of the fixed wall on the pebble packing structures and purge gas flow characteristics was investigated by combining the discrete element method (DEM) and computational fluid dynamics (CFD) method. The results indicate that the fixed wall leads to a regular packing of the pebbles adjacent to the fixed wall in association with drastic fluctuations in the porosity of the pebble bed, which can affect the purge gas flow behaviors. Further analyses of helium flow behaviors show that the helium pressure in the pebble bed decreases in a linear manner along the flow direction, whereas the pressure drop gradient of helium increases gradually with an increase in the packing factor. The reduction in porosity in the pebble bed leads to a notable escalation in helium flow velocity. Concerning the direction perpendicular to the helium gas flow, the evolution of the cut-plane averaged velocity of helium is similar to that of the porosity, except in the region immediately adjacent to the wall. The pressure drop and flow characteristics obtained in this study can serve as input for the thermohydraulic analysis of the tritium blowing systems in the tritium-breeding blanket of a fusion reactor.

Keywords: pebble bed; flow characteristic; helium gas; pressure drops; DEM-CFD



Citation: Gong, B.; Cheng, H.; Zhou, B.; Yan, J.; Wang, L.; Zhang, L.; Feng, Y.; Wang, X. Investigation of Wall Effect on Packing Structures and Purge Gas Flow Characteristics in Pebble Beds for Fusion Blanket by Combining Discrete Element Method and Computational Fluid Dynamics Simulation. *Appl. Sci.* **2024**, *14*, 2289. <https://doi.org/10.3390/app14062289>

Academic Editor: Francesca Scargiali

Received: 27 December 2023

Revised: 4 March 2024

Accepted: 5 March 2024

Published: 8 March 2024



Copyright: © 2024 by the authors. Licensee MDPI, Basel, Switzerland. This article is an open access article distributed under the terms and conditions of the Creative Commons Attribution (CC BY) license (<https://creativecommons.org/licenses/by/4.0/>).

1. Introduction

Tritium is the primary nuclear fuel for deuterium–tritium fusion reactors. However, tritium’s reserves in nature are so small, they are almost negligible. Therefore, to maintain the continuity of the fusion reactor, production of tritium through the tritium-breeding blanket in a fusion reactor is required [1]. In the tritium-breeding blanket, tritium is bred via the $\text{Li}(n, \alpha)^3\text{H}$ reaction between lithium atoms and neutrons in tritium breeder materials [2,3]. The lithium ceramic pebbles are always selected as breeder materials, such as Li_4SiO_4 and Li_2TiO_3 pebbles, which are packed in cavities of tritium-breeding blankets and formed fixed beds [4,5]. For example, the Li_4SiO_4 pebbles with diameters of ~1 mm are utilized in the helium-cooled ceramic breeder (HCCB) blanket [2,6].

In the tritium-breeding blanket, when the produced tritium is released into the pores of the bed, the tritium needs to be carried out of the bed by the purge gas and then into the tritium extraction system (TES) for further processing [7,8]. However, the efficiency of tritium extraction is affected by the flow characteristics of purging gas. Additionally, the gas flow behaviors are influenced by the pebble packing structure and the operating conditions of the fluid. Therefore, it is crucial to comprehensively investigate flow behaviors and characteristics of the tritium-purging gas for the design and operation of the tritium-breeding blanket in a fusion reactor.

The flow characteristics of the tritium-purging gases are primarily characterized by pressure drop and flow rate at the macroscopic level. Abou-Sena et al. [9,10] experimentally measured the helium gas pressure drops in cylindrical and rectangular pebble beds at the macroscopic level and analyzed the influences of the pebble size, bed length, and inlet velocity on the pressure drop in pebble beds. Wang et al. [11] and Liu et al. [12] measured the pressure drop of helium gas in beds packed with stainless steel pebbles of 0.5~2 mm with focus on the influence of pebble size. The results show that reducing the particle size can reduce the porosity and increase the pressure drop. Panchal et al. [13] evaluated the pressure drop of nitrogen gas in particle beds with different materials and pebble sizes. Their findings indicated that the pressure drop increases as pebble diameter decreases and velocity increases, which are consistent with the Ergun model with modified Ergun constant. The aforementioned experimental results are crucial in the design of solid tritium-breeding blanket. However, experimental measurements can only provide the macroscopic pressure drops and cannot discern the intricate flow characteristics of the localized pebble bed.

At the fine-particle-scale level, flow behaviors are manifested as local pressure, flow and velocity distribution, along with local flow characteristics, which are always explored by numerical simulation. Chen et al. [14] conducted numerical studies on the properties of helium gas flow in unary-sized and binary-sized pebble beds, providing a detailed analysis of pressure distribution and velocity variation, and obtained the porosity distribution and velocity and pressure field distributions in binary-sized pebble beds. Wu et al. [15] explored the impact of bed scale on the flow characteristics of purge helium gas in small pebble beds with various column-to-pebble diameter ratios. The results indicate that the wall effect on the packing structures and flow characteristics cannot be neglected in small pebble beds. For different-order and randomly pebble packed beds, Chen et al. [16] examined the effects of the order packing structures and random packing structures on the pressure distribution and velocity distribution, and obtained the loss coefficient of helium through the pebble bed with different packing structures. Meanwhile, Zhou et al. [17] investigated the heat transfer properties between Li_4SiO_4 pebbles and the helium gas. The results show that the temperature of purge gas will rapidly rise from 20 °C to 500 °C as the purge gas flows into the pebble bed. For the packed pebble beds with different pebble sizes and pebble properties, Choi et al. [18] and Lee et al. [19] examined the influence of particle size distribution and packing factor on helium flow behavior in pebble beds. The results show that the pressure drop increases not only in proportion to packing factor, but also in inverse proportion to the difference in pebble size. Lei et al. [20] analyzed the friction coefficient of the packing structures and gas flow behaviors of ceramic pebble beds. Their finding indicates that the pressure drop gradually increases with the decrease in the friction coefficient between pebbles. Zhang et al. [21] modeled the purge behaviors of helium gas in breeder pebble beds and analyzed the distribution of tritium within the beds. The results show that the velocity has the same damped oscillating profile with radial porosity distribution. Sedani et al. [22] conducted numerical and experimental investigations on the flow behaviors of nitrogen and helium gasses in pebble beds. The results demonstrate that localized packing structures can significantly affect the flow characteristics of helium in pebble beds. The above numerical investigation explored the effects of particle size, pebble bed size, temperature distribution, and friction coefficient on the packing behaviors and helium flow characteristics of the pebble bed. However, there is a significant lack of research on the purge gas flow characteristics inside the pebble bed under different wall conditions in the solid tritium-breeding blanket of a fusion reactor.

In this study, the effects of fixed walls on the packing structures and flow characteristics of purge gas helium in pebble beds are investigated numerically by combining DEM and CFD methods, which results in an effective tool for simulating the heat and mass transfer in particle packed bed [15,18]. The pebble packing method based on the DEM simulation as well as the methodology of building a model, mesh-independent analysis and simulation setups based on CFD simulation are introduced in Section 2. In Section 3, the detailed

packing structures and flow characteristics, such as packing factor and porosity, pressure distribution, and velocity distribution are obtained. These results are discussed in detail in Section 3. Finally, some conclusions are summarized in Section 4.

2. Numerical Methodology

The particle packing is a complex process involving a large number of multi-body collisions and particle interactions. The discrete element method can simulate well the interaction between each particle and obtain the closest state to that of the actual physical particle packing, which have been demonstrated in a large number of studies in the literature [5,23–27], particularly on the use of DEM to simulate a particle packing process. In addition, it is well known that CFD calculations can simulate the flow behavior of fluids and obtain detailed information about fluid behaviors, such as pressure distribution and velocity distribution.

Firstly, DEM modeling is used to simulate the particle random packing process and establish a fixed pebble bed model with random packing of pebbles. Then, by transferring the pebble bed data and reconstructing the physical geometry, the CFD model can be built. Finally, the gas flow characteristics inside the pebble bed can be obtained by using the CFD solution. By combining the two methods, DEM and CFD, it is possible to obtain the characteristics of the fluid flow behavior in the internal pores of the pebble bed that are closest to the real particle packing state. It provides an excellent way to evaluate the detailed flow characteristics of the purge gas helium inside the tritium breeder pebble bed of a fusion blanket. In addition, this approach of using a combination of DEM and CFD to study gas flow within a fixed bed of particles has been used in a large number of applications in other chemical industries [15,22,28–31].

Therefore, in this study, a one-way coupling of DEM and CFD is utilized to model the pebble packing process and solve the helium gas flow behaviors in the porous of randomly packed pebble beds. Figure 1 shows the flowchart of the simulation process, as follows:

- Section I: DEM simulation was used to model the pebble packing process and to obtain the pebble bed model of the specific packing structures. To start DEM modeling, firstly, the parameters of bed dimension, pebble material properties, pebble size, pebble distribution, etc., should be determined. Then, gradually insert pebbles into the bed container by the gravity falling rain method. The pebbles fall down and become packed in the container. When a specific bed height is reached or a specific number of pebbles are inserted, the pebble inserting process is stopped. The pebbles gradually reach a stable state through energy dissipation. Finally, the pebble bed model with a specific packing structure is obtained. Then, the pebble bed model data are passed to the CFD software (ANSYS CFX 2019R2) through a coupling interface program.
- Section II: CFD simulation was adopted to model the purge gas flow behaviors of helium in the void structure of the pebble beds. At first, the pebble bed model is regenerated and established after obtaining the pebble bed data, which were transferred from the VB interface program. The point of contact between the pebbles makes it difficult to mesh; therefore, a handling of contact point is necessary. Then, the fluid domain is meshed. After setting the boundary conditions for fluid computation, the numerical solution can be performed. Finally, the pebble bed flow field data are obtained and post-processing of the simulation results can be performed to obtain detailed flow characteristics of helium in pebble beds.

The pebble packing process is simulated by the DEM. In this method, each pebble is treated as a separated element. By the Hertz–Mindlin contact theory [32], the contact force between two touched particles is calculated. After applying the gravity and contact force on each pebble, the particles' motion can be simulated by solving Newton's second law of motion. The position, velocity, contact force, contact state, etc., can be obtained and updated at each time-step.

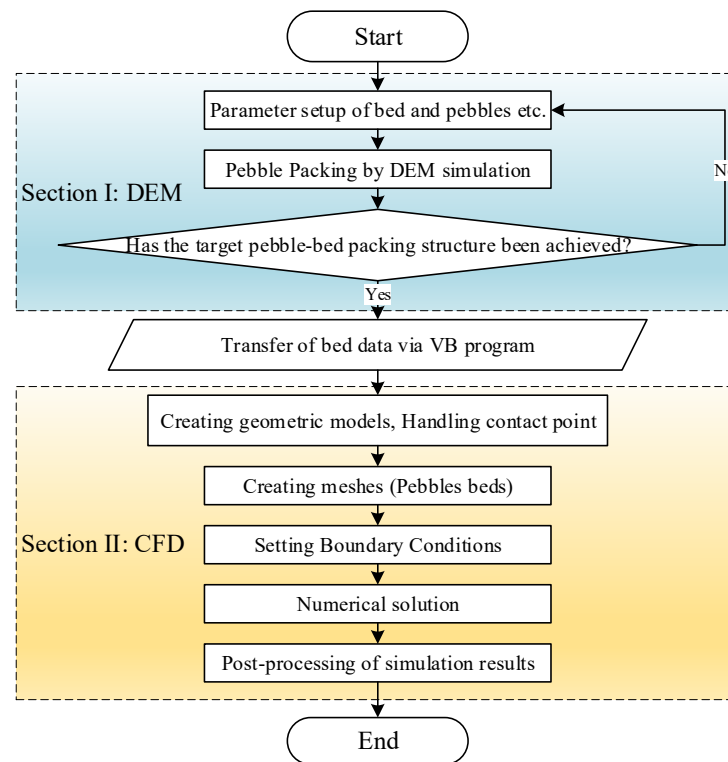


Figure 1. Flow chart of the simulation process by combining DEM and CFD modeling.

2.1. Pebble Packing by DEM

During the pebble packing process, the pebble motion can be expressed as the following equations:

$$m_i \frac{dV_i}{dt} = \sum_{j=1}^{N_{cn}} (F_{n_{ji}} + F_{t_{ji}}) + m_i g \quad (1)$$

$$I_i \frac{d\omega_i}{dt} = \sum_{j=1}^{N_{cn}} r_{ij} \times F_{t_{ji}} \quad (2)$$

where V_i and ω_i are the velocity of the translational and rotational movements of pebble i , respectively. m_i and I_i are the pebble mass and the motion of inertia. N_{cn} is the number of surrounding pebbles. F_n and F_t are normal and tangential contact forces between two touched pebbles. F_g is the gravity force. r_{ij} is the vector pointing from the pebble i to pebble j . Under the influence of the friction between two pebbles, the normal contact force and the tangential contact force satisfy $|F_t|_{max} \leq \mu_{fri} |F_t|$, where μ_{fri} is the friction coefficient.

Based on the Hertz–Mindlin [32] contact theory, F_n and F_t can be defined as follows:

$$F_n = k_n \delta_{n_{ij}} - \eta_n v_{n_{ij}} \text{ and } F_t = k_t \delta_{t_{ij}} - \eta_t v_{t_{ij}}. \quad (3)$$

For normal contact force, k_n is the elastic constant of normal contact; η_n is the normal viscoelastic damping coefficient. $\delta_{n_{ij}}$ is the overlap of two normal contact pebbles. $v_{n_{ij}}$ is the normal relative velocity of two pebbles. k_n and η_n can be expressed as

$$k_n = \frac{4}{3} E^* \sqrt{R^* \delta_{n_{ij}}} \text{ and } \eta_n = -2 \sqrt{\frac{6}{5}} \beta \sqrt{S_n m^*} \quad (4)$$

where $S_n = 2E^* \sqrt{R^* \delta_{n_{ij}}}$, $\eta_n \geq 0$.

For tangential contact force, k_t is the elastic constant of tangential contact; η_t is the tangential viscoelastic damping coefficient. $\delta_{t_{ij}}$ is the tangential relative displacement vector

of two contact pebbles. $v_{t_{ij}}$ is the tangential relative velocity of two pebbles. k_t and η_t can be shown as

$$k_t = 8G^* \sqrt{R^* \delta_{t_{ij}}} \text{ and } \eta_t = -2\sqrt{\frac{6}{5}} \beta \sqrt{S_t m^*} \tag{5}$$

where $S_t = 8G^* \sqrt{R^* \delta_{n_{ij}}}$, $\eta_t \geq 0$. $\beta = \frac{\ln(e)}{\sqrt{\ln^2(e) + \pi^2}}$.

For the above formulas, Y^* , G^* , m^* , and R^* are the effective elastic modulus, the effective shear modulus, the equivalent mass, and the equivalent radius of two contact pebbles, respectively. The DEM simulation was conducted by using the LIGGGHTS code [33]. The detailed description of the DEM theory can be found in the referenced literature [34].

To simulate the pebble real packing process under gravity, the falling rain method was used in this paper. The main pebble packing process is shown in Figure 2. Initially, pebbles are randomly generated in the top region of the bed before being allowed to move freely under gravity. These pebbles then gradually fall and eventually pack at the bottom of the bed, as shown in Figure 2a. Finally, to flatten the packing of pebbles at the top surface of the pebble bed and assist in determining its height, pebbles above a specific height are removed, as shown in Figure 2b. The pebble bed undergoes a compression and release process with a minimal load, illustrated in Figure 2c. The algorithm takes into consideration the contact force between particles, gravity, frictional, and collisional interactions, and closely mimics the physical process of pebble packing. Consequently, it effectively simulates the random pebble packing process in a pebble bed.

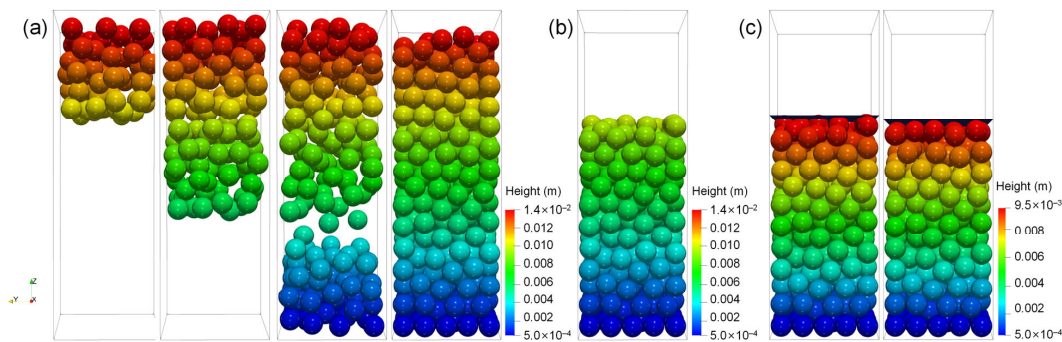


Figure 2. Pebble packing process under gravity by DEM simulation: (a) packing process, (b) deleted pebbles, (c) compression.

In this study, Li_4SiO_4 ceramic pebbles were selected in the DEM simulation. The specific characteristics of Li_4SiO_4 pebbles implemented in DEM are outlined in Table 1. Specific values were referenced from the literature [35]. The final bed dimension is $5d \times 5d \times 10d$ (length of pebble beds, H , is $10d$) with four different boundary conditions. When 4 walls of the boundary are applied, 4 lateral walls of the bed container become fixed walls. When 2 walls and 2 periodic boundaries are applied, the boundary condition is as shown in Figure 3. When 4 periodic boundaries are applied, there are no lateral walls in the container. Finally, 259, 279, and 295 pebbles were packed in the container. The detailed information of the pebble beds is listed in Table 2.

Table 1. Properties of pebble materials used in DEM.

Property	Symbols	Value [35]
Density (kg/m^3)	ρ_p	2323
Young's modulus (GPa)	E	90
Poisson ratio	ν	0.24
Friction coefficient	μ_{fri}	0.1
Restitution coefficient	e	0.9
Pebble diameter (mm)	d	1

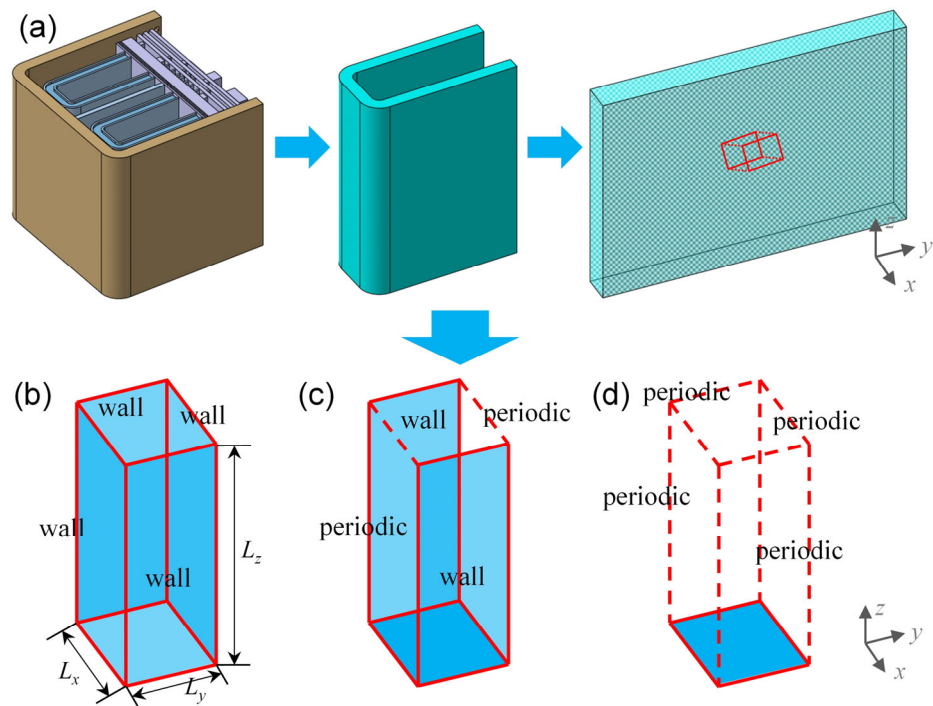


Figure 3. Pebble beds in (a) simplified cavities of HCCB TBM and three boundary conditions, (b) 4 fixed walls, (c) 2 fixed walls and 2 periodic boundaries, and (d) 4 periodic boundaries.

Table 2. Bed properties of pebble materials used in DEM.

Cases	Bed Dimension	Boundary Condition	Pebble Number, N
1	$5d \times 5d \times 10d$	4 walls	259
2	$5d \times 5d \times 10d$	2 walls and 2 periodic boundaries	279
3	$5d \times 5d \times 10d$	4 periodic boundaries	295

2.2. Pebble Bed Physical Model

After the DEM simulation, the pebble bed data, such as particle coordinates, particle diameters, pebble bed dimensions, and contact point, are transferred to the CFD software through the VB coupling interface program to regenerate the pebble bed geometry model. Due to the intricate geometry of the void flow channel in a randomly packed bed, a finer mesh is usually required to improve the accuracy of the CFD simulation. However, a finer mesh will inevitably consume a large number of computational resources. Therefore, a small-scale pebble bed or localized pebble bed is usually used in the particle-resolved CFD simulation in pebble beds. However, the fixed walls of small-sized pebble beds have a significant effect on the packing structure, which will inevitably affect the gas flow characteristics inside the pebble bed.

In addition, in HCCB TBM, the breeder pebbles are packed in u-shaped cavities [2], as shown in Figure 3. The majority of the breeder pebble beds can be simplified as rectangular pebble beds. However, the simplified full-scaled pebble bed is still huge for particle-resolved CFD simulation. It is necessary to use a localized pebble bed model for the simulation of purge gas flow behaviors. To investigate the impact of walls on flow behaviors in a localized pebble bed, three kinds of simplified bed boundary conditions are selected, as shown in Figure 3. Therefore, in this study, three different wall conditions of the pebble beds are used to establish the pebble bed models. The helium flow characteristics inside these three pebble beds are focused on and analyzed to assess the impact of the wall effect on the gas flow characteristics of beds. Figure 4 shows the pebble bed model that is randomly packed with various boundary conditions. In Figure 4a, four fixed walls are adopted in

the small-scale pebble bed. Figure 4b shows the pebble bed with two fixed walls and two periodic boundaries, which can represent a pebble bed between two infinite parallel walls. Furthermore, the use of four periodic boundaries is demonstrated in Figure 4c, which eliminates the influence of fixed walls on pebble packing and approximates an infinitely sized pebble bed packed randomly.

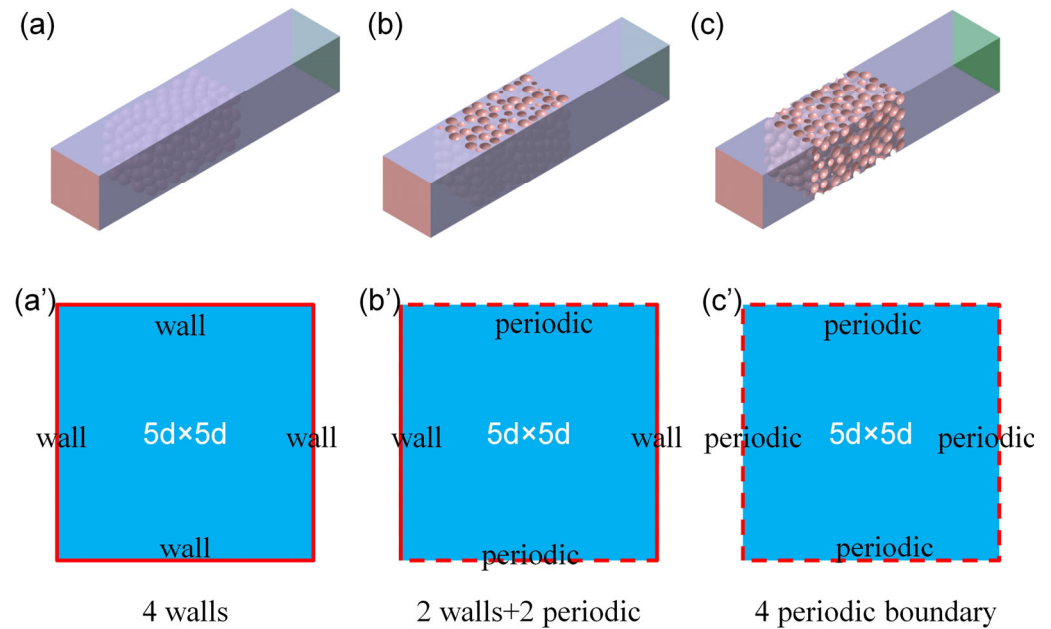


Figure 4. Pebble bed models with different walls and boundaries: (a) model and (a') boundaries with 4 fixed walls, (b) model and (b') boundaries with 2 fixed walls and 2 periodic boundaries, and (c) model and (c') boundaries with 4 periodic boundaries.

2.3. Contact Point Handling

The geometrical distortion near the contact point between pebbles will cause difficulties in the meshing process and reductions in grid quality; the contact points need to be processed to obtain suitable meshes and ensure simulation accuracy [36]. Calis et al. [37] investigated the influence of reduction method on pressure drop in beds. Results indicate that the error of the simulation results is within 0.5% when the contact points are treated by the reduction method and the particle diameters are reduced to 98%*d* and 99%*d*, which have a very small effect on the simulated gas flow characteristics. In addition, Chen et al. [14] and Lei et al. [20] used CFD to simulate the purge gas flow characteristics in pebble beds by reducing the particle diameter to 98%*d* and obtained reasonable simulation results. Therefore, in this study, the pebble diameters were reduced to 98%*d*. The processed pebble bed model will be used in CFD simulation. The influence of the reduction in pebble diameter on packing structures will be discussed in Section 3.1.

2.4. Mesh Independence

After the handling of the contact point between pebbles, the fluid domains in the pebble bed are meshed. In our previous investigation [16], the flow characteristics of purge gas helium in the order and randomly packed pebble beds were analyzed by the ANSYS CFX. Similar to that in reference [16], the mesh independence was conducted in the analysis of the pressure drop of helium in a pebble bed with BCC order packing.

A constant physical isothermal flow of helium (He) at 300 °C was used as the fluid medium. Helium density was 0.2518 kg/m³, and kinetic viscosity was 3.0705×10^{-5} kg/m·s. Owing to the fact that the inlet velocity of helium in a tritium breeder pebble bed is in the range of 0.1~0.2 m/s, the laminar flow model was selected for steady state calculations [16,18]. Inlet velocity and outlet pressure conditions were adopted in this study. The inlet flow velocity, v_i ,

was 0.1 m/s. The outlet relative pressure, P_o , was 0 Pa. The ambient base pressure, P_a , was set to be 0.3 MPa. Finally, six sets of meshes with different mesh scales of $9.8 \times 10^5 \sim 1.59 \times 10^7$ were meshed and analyzed. The local mesh distributions are displayed in Figure 5. The pressure drop gradient in the order packed pebble bed with different mesh scales are presented in Figure 6. The deviation between the marked mesh (~ 7.46 million) and the finer one (~ 10.1 million) was smaller than 0.17%. That is to say, when the number of meshes was greater than 7.46 million, the simulation results tended to stabilize. Thus, the settings of the marked mesh, as marked by the red circle in Figure 6, were selected and applied to the other simulation in this work.

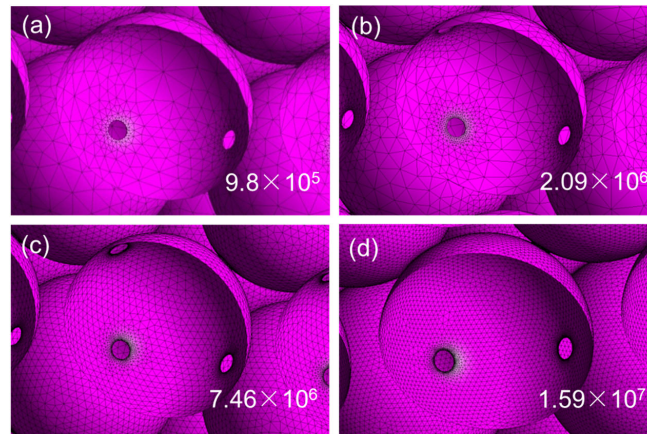


Figure 5. Local mesh distribution with different mesh scales: (a) 9.8×10^5 , (b) 2.09×10^6 , (c) 7.46×10^6 , (d) 1.59×10^7 .

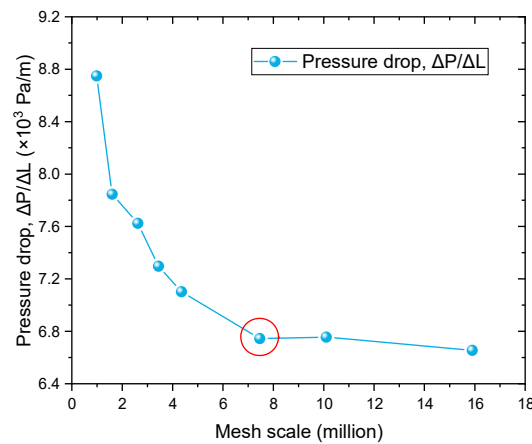


Figure 6. Pressure drop of helium in order packed pebble beds with BCC packing.

2.5. CFD Simulation and Parameter Settings

In this work, the incompressible flow of helium (He) at 300 °C (helium density is 0.2518 kg/m³, dynamic viscosity is 3.0705×10^{-5} kg/m·s) was used as the fluid medium. The energy equation was not considered in our CFD model. Thus, the governing equations of the continuity equation and the momentum equation is as follows:

$$\frac{\partial \rho}{\partial t} + \nabla \cdot (\rho U) = 0 \tag{6}$$

$$\frac{\partial (\rho U)}{\partial t} + \nabla (\rho U \otimes U) = -\nabla p + \nabla \cdot \tau, \tag{7}$$

where ρ is the density of fluid. U is the velocity of fluid. The stress tensor, τ , is related to the strain rate by

$$\tau = \mu \left(\nabla U + (\nabla U)^T - \frac{2}{3} \delta \nabla \cdot U \right). \quad (8)$$

where μ is the dynamic viscosity of the fluid.

Based on the pebble bed configurations gained in DEM simulation, a CFD model of the bed is reconstructed as shown in Figure 7. In the CFD model, the ceramic pebbles are assumed to be fixed, owing to the one-way coupling framework used in this work. By referring to another study [18], the laminar flow of the purge gas helium in the pebble bed was considered in the simulation. In addition, inlet velocity and outlet pressure conditions are adopted in this study. The inlet flow velocity, v_i , is 0.1 m/s. The outlet relative pressure, P_o , is 0 Pa. The ambient base pressure, P_a , is set to be 0.3 MPa. In addition, the slip boundaries are adopted in the periodic boundaries of the pebble bed. The fixed walls and pebble surfaces are set as the non-slip wall. In order to achieve a stable flow field and avoid the occurrence of reflux and end-wall effects, the inlet and outlet of the pebble bed are extended for 5 d and 10 d, respectively, as shown in Figure 7. Then, the numerical solution is carried out to obtain the flow characteristics of the pebble bed. Finally, the post-processing of the simulation results is carried out.

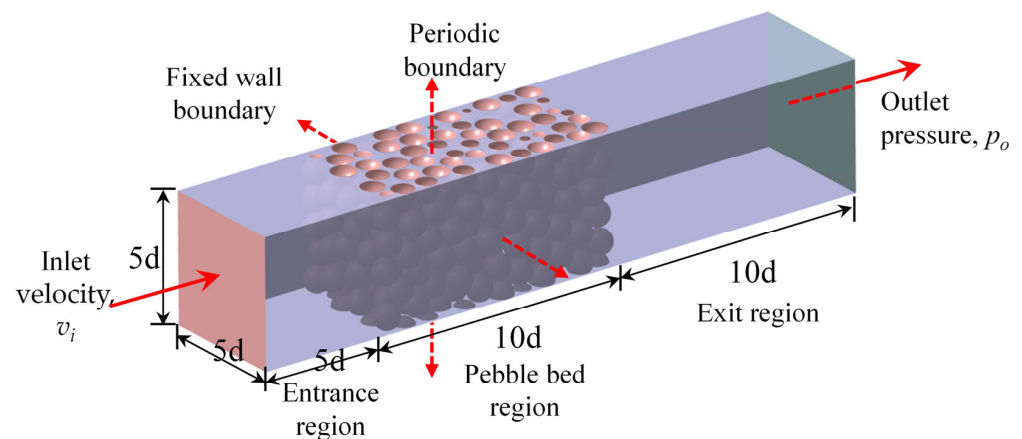


Figure 7. Reconstructed pebble bed geometric model.

In this study, the CFD simulations were performed in the commercial software ANSYS CFX 2019R2. The pressure loss along the flow direction of the pebble beds was obtained by the averaged values of the cross-sectional plane perpendicular to the flow direction. The detailed theoretical equations can be referred to from the literature [38]. To obtain the converged solutions at steady state, all CFD simulations were conducted until the residuals of the continuity and momentum equations became less than 10^{-5} .

3. Results and Discussions

3.1. Wall Effect on Packing Structures

Fixed walls can significantly impact the packing characteristic of a pebble bed. The average packing factor of these pebble beds with different wall boundary conditions are shown in Figure 8. The results show that the smallest packing factor was observed in the pebble bed with four fixed walls. Utilizing four periodic boundaries in the pebble bed resulted in a higher packing factor and lower porosity. Therefore, as the quantities of fixed wall decreases, the packing factor increases and the porosity decreases. Compared to the pebble bed with four fixed walls, the average packing factor of the pebble beds with four periodic boundaries increased by 18.58% to 0.6178. This is mainly due to the lower packing factor of the pebble bed in the region close to the fixed wall. An increase in the number of fixed walls will increase the fixed wall's affected regions, which leads to a lower packing factor of the pebble bed.

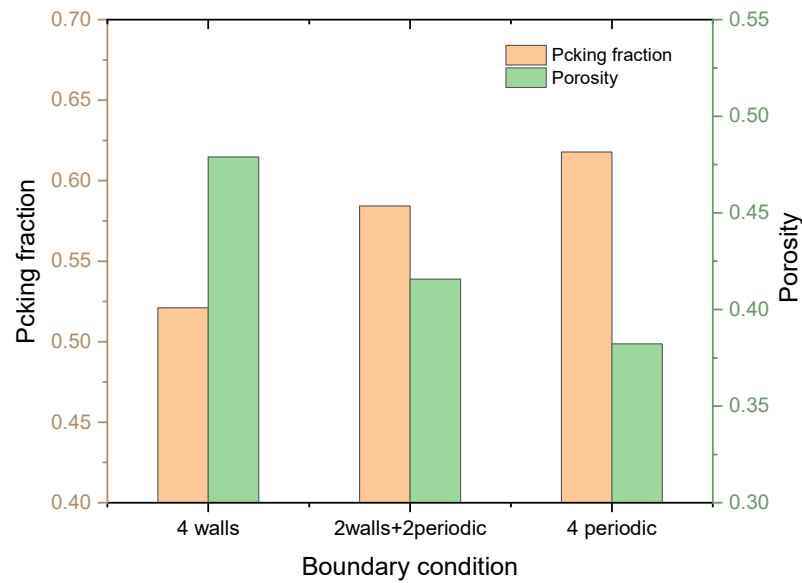


Figure 8. Packing factor of pebble beds with different boundary walls.

To investigate this phenomenon, the distribution of localized packing factors of the pebble bed in the x–y plane is calculated for different wall and boundary conditions, respectively, as presented in Figure 9. The figures show that the fixed walls have a notable influence on the local packing factor distribution. In the pebble bed with four walls, several areas near the wall exhibit high localized packing factor, resembling “hot spots”. The corners feature greater localized packing factors as an effect of the double walls, whereas the inner regions of the pebble bed showcase more uniformly distributed packing factors. In the pebble bed with two fixed walls and two periodic boundaries, a high localized packing factor is found only near the parallel fixed walls. Meanwhile, the distribution of localized packing factor is more uniform in the inner region of the pebble bed and near the periodic boundary. As for the pebble bed with four periodic boundaries, the distribution of local packing factor is more uniform throughout the entire pebble bed. The observed distributions stem from the fact that pebble packing adjusts to the structure of a fixed wall, leading to a partially regular or layered distribution near the fixed wall. This is demonstrated in Figure 9a’–c’, which exhibit similar distribution characteristics in the centers of the pebbles, while in the middle region of the pebble bed and the regions close to the periodic boundary, the influence of the fixed wall on the packing structure gradually decreases and the packing structures gradually become random and homogeneous.

In addition, the area-averaged axial packing factors along different axial directions are calculated for the initial bed obtained by DEM simulation and the bed after a reduction in pebble diameter to 0.98d; the results are shown in Figure 10. Similar evolutionary patterns are observed in the pebble bed before and after reductions in pebble diameter. The effect of pebble diameter reduction on the packing factor distribution of the pebble bed is minimal.

To validate the physical model of pebble beds established by using DEM simulations, the axial packing factor distribution near the wall was analyzed in comparison with the calculated results of the empirical model proposed by Klerk based on the experimental results [39]. Klerk’s empirical model is shown as follows:

$$\varepsilon(x) = \begin{cases} 2.14x^2 - 2.53x + 1 & (\text{if } x \leq 0.637) \\ \varepsilon_b + 0.29 \cos(2.3\pi(x - 0.16)) \times e^{-0.6x} + 0.15e^{-0.9x} & (\text{if } x > 0.637) \end{cases} \quad (9)$$

where $\varepsilon(x)$ is the local porosity; packing factor $\gamma(x) = 1 - \varepsilon(x)$. x is the non-dimensional distance to the fixed wall. ε_b is average porosity in the inner bulk region of the pebble bed.

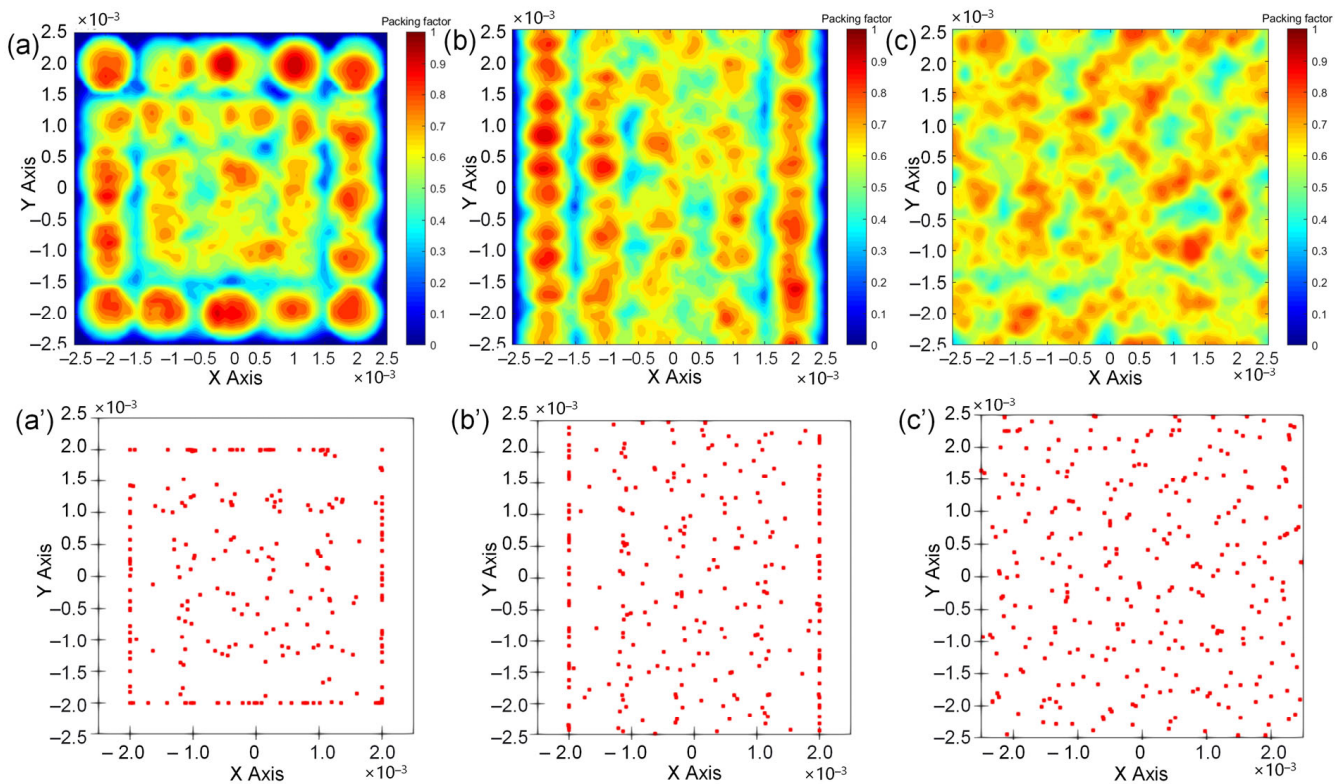


Figure 9. Porosity and pebble center distribution in pebble beds with (a,a') 4 fixed walls, (b,b') 2 fixed walls and 2 periodic boundaries, and (c,c') 4 periodic boundaries.

Figure 10a,b,d show a decaying oscillation in the axial packing factor in the direction perpendicular to the wall (x - or y -axis) caused by the presence of a fixed wall in both initial beds and processed beds. The results in this study are consistent with the Klerk empirical model [39]. Figure 10e,g,h show that the packing factor is more uniformly distributed without violent oscillations due to the use of periodic boundaries in the y -axis without the presence of fixed walls. This demonstrates that the pebble bed model attained through DEM simulation in this work is in agreement with the actual pebble bed, which can reflect the actual random packing structure of the pebble bed. Additionally, Figure 10c,f,i illustrate the axial packing factor distribution along the vertical (z -axis) direction, revealing that the packing factor oscillations occur in the top and bottom regions. The observed phenomenon stems from the packing of particles in the bottom wall area and the very low load compression in the pebble bed. Moreover, axial packing factor oscillations persist in the middle pebble bed region, attributable to the significant wall effect at a distance of $5d$ from the wall [40]. In this paper, the pebble arrangements within the central region of the pebble bed remains influenced by the side wall effect.

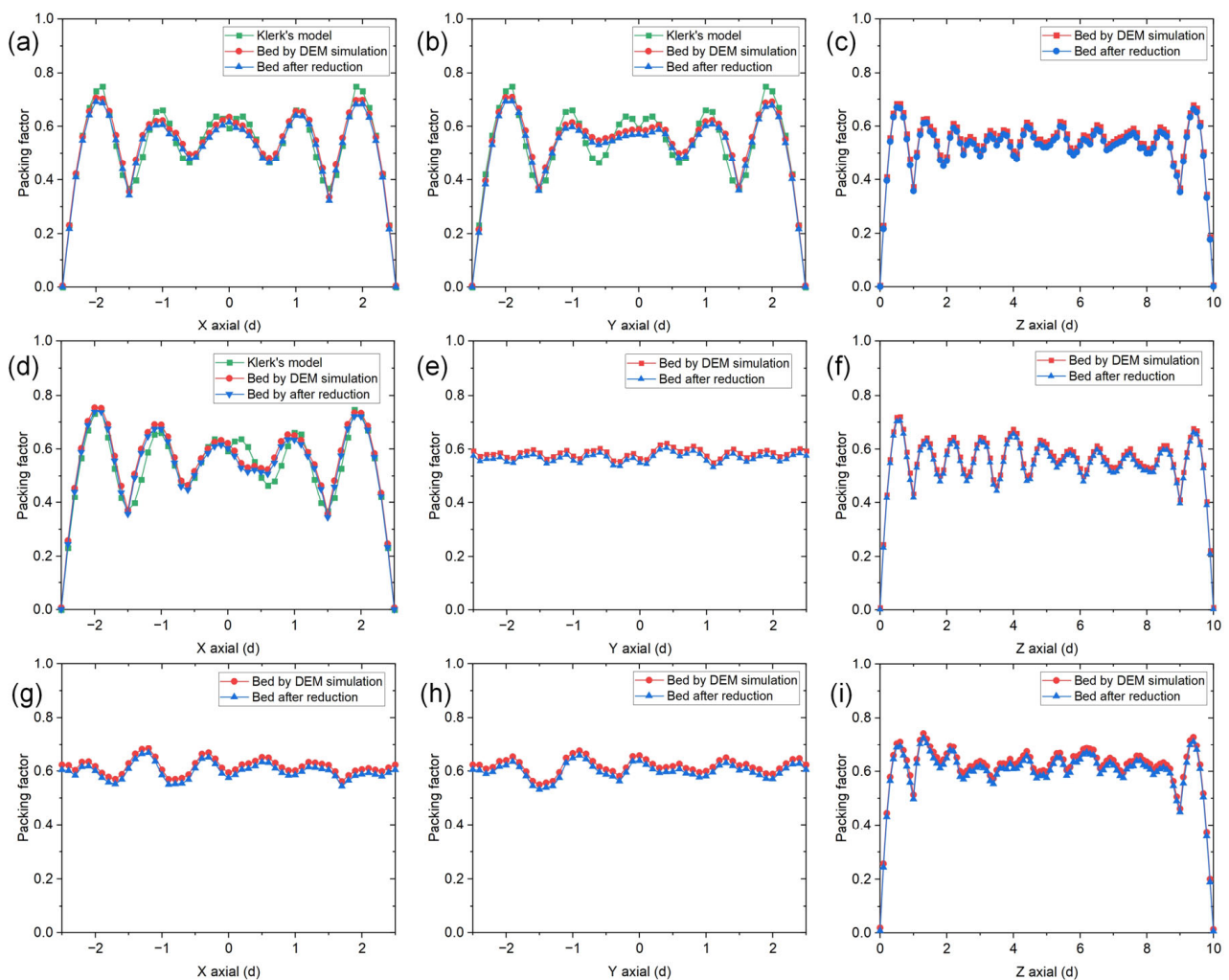


Figure 10. Axial packing factor variation in pebble beds with (a–c) 4 fixed walls, (d–f) 2 fixed walls and 2 periodic boundaries, and (g–i) 4 periodic boundaries.

3.2. Wall Effect on Pressure Distribution

To investigate the affecting mechanisms of the wall effect on the pressure distribution in randomly packed pebble beds, the helium gas flow behaviors in randomly packed pebble beds were numerically investigated. The detailed data of the helium flow in the pebble bed are obtained by the steady state simulation. Figure 11 illustrates the pressure distribution inside the pebble bed with three different wall boundaries. Figure 11a–c display the pressure distribution inside the pebble bed and on the surface of the pebbles, while Figure 11a'–c' reveal the pressure distribution in the mid-plane of the pebble bed. The findings demonstrate that the pressure distribution is uniform with minimal variation before helium enters the pebble bed. As helium passes through the bed, the helium pressure progressively decreases. Although there is a slight difference in local pressures due to the void distribution within the pebble bed, the pressures exhibit a gradual decline in the flow direction. Following the helium gas discharge from the pebble bed, the pressure promptly reverts to a uniform distribution, with its value gradually approaching the outlet pressure.

In order to quantitatively analyze the along-travel pressure drop along the flow direction within three types of pebble beds, the averaged pressures of the cross-sectional plane were calculated at different positions along the flow direction. The resulting data are presented in Figure 12a, indicating minimal variance in helium pressure prior to entering the pebble bed. After the fluid passes through the pebble bed, the pressure decreases linearly. As it exits the pebble bed, the pressure rapidly stabilizes and reaches equilibrium

with the relative pressure at the outlet position. This is mainly due to the fact that the pebble packed bed is a porous medium. As the helium passes through the pebble bed, it encounters resistance, resulting in pressure loss, which is closely related to the characteristics of the pebble bed porous media.

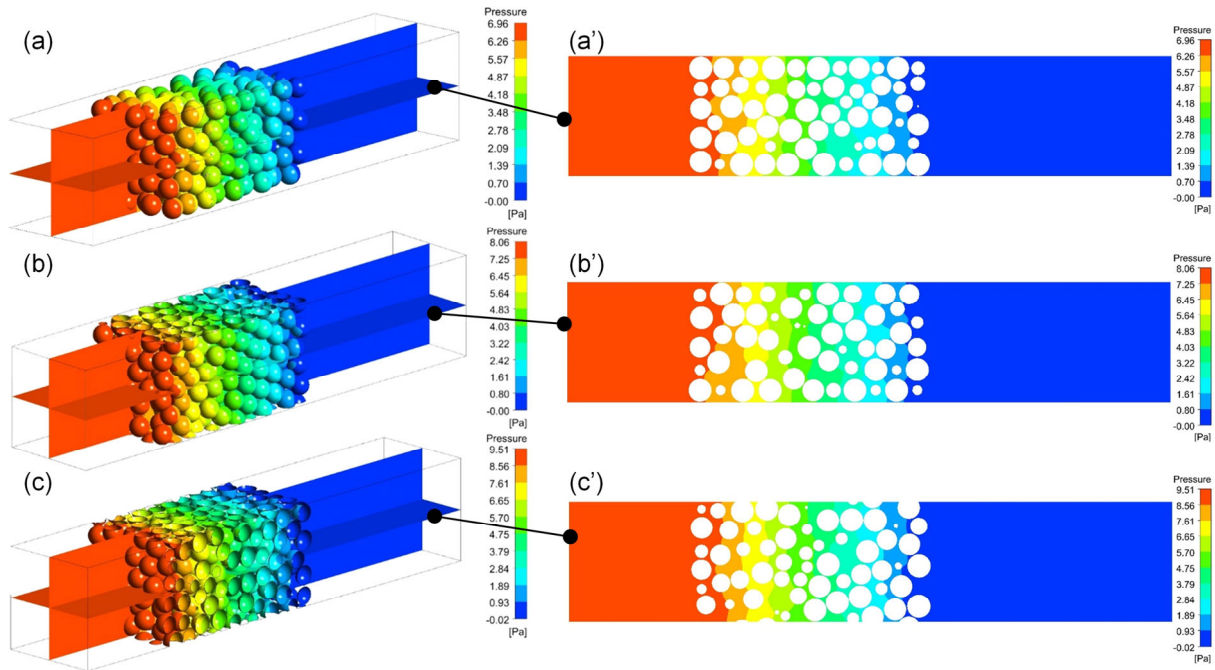


Figure 11. Pressure distribution in pebble beds with different boundaries: (a) 3D view and (a') midplane distribution with 4 fixed walls, (b) 3D view and (b') midplane distribution with 2 fixed walls and 2 periodic boundaries, and (c) 3D view and (c') midplane distribution with 4 periodic boundaries.

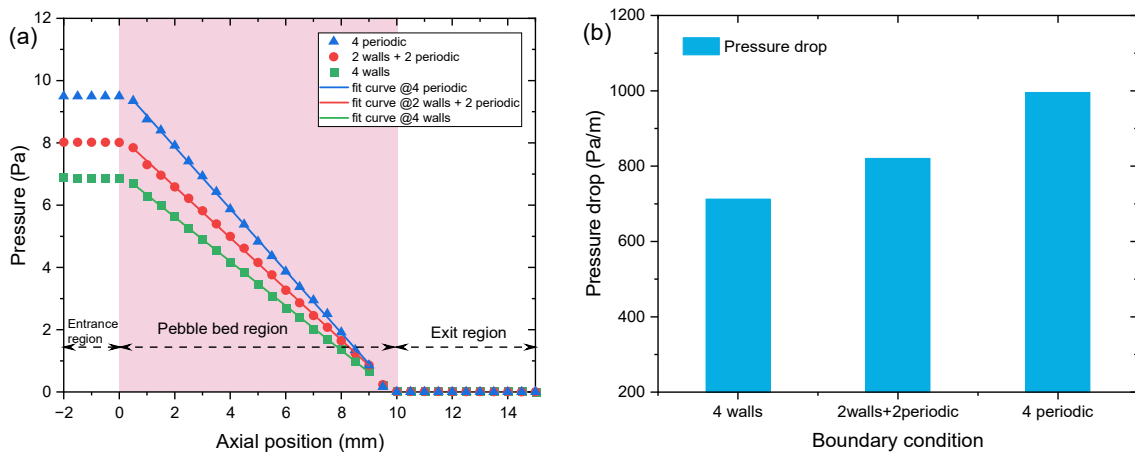


Figure 12. Pressure distribution in pebble beds with different boundaries: (a) along the flow direction, (b) pressure drop per unit length.

Additionally, the pressure drop gradient can be obtained by linearly fitting the cross-sectional averaged pressure loss over the pebble bed position after entering the pebble bed regions, as follows:

$$\begin{aligned}
 y &= -0.71238x + 7.0389, @ 4 \text{ walls}, \\
 y &= -0.82072x + 8.2351, @ 2 \text{ walls and } 2 \text{ periodics}, \\
 y &= -0.99546x + 9.8626, @ 4 \text{ periodics}.
 \end{aligned}
 \tag{10}$$

where x is in mm, y is in Pa. Finally, the pressure drop gradient of helium in pebble beds are 712.83 Pa/m, 820.72 Pa/mm, and 995.46 Pa/m, respectively, with three different wall boundaries. Figure 12b displays the helium pressure drop gradient in pebble beds with different wall boundaries. It is evident that the pressure drop gradient is the least for the pebble bed with four fixed walls, while the pebble bed with the four periodic boundaries experiences the greatest pressure drop gradient. The pressure drop gradient in the pebble bed, featuring two fixed walls and two periodic boundaries, falls between the pressure drop gradient in pebble beds comprising four fixed walls or four periodic boundaries. Compared to the pebble bed with four fixed walls, the pressure drop gradient of helium in the pebble beds with four periodic boundaries increased by 39.73% to 995.46 Pa/m. This is primarily because various wall boundary conditions alter the packing structure of randomly packed pebble beds. The impact of the fixed walls on the packing structure of pebble beds decreases gradually as the quantity of fixed walls diminishes. As indicated by Figure 8, utilizing four periodic boundaries in the pebble bed results in a higher packing factor and lower porosity. Therefore, as the quantities of fixed wall decreases, the packing factor increases, the porosity decreases, and the pressure drop gradient of helium in bed increases gradually. In addition, it can also be seen from Table 2 that as the number of fixed walls decreases, the number of pebbles filled in the pebble bed gradually increases. The total surface area of the pebbles inside the pebble bed gradually increases, leading to more pressure loss due to the friction between the helium and the pebble surfaces.

3.3. Wall Effect on Velocity Distribution

To analyze in greater detail the flow characteristics of helium inside the pebble bed, separate calculations were made for the cross-sectional average velocities of helium at various locations along the flow direction of the bed. These calculations are illustrated in Figure 13a. The results indicate that the velocity of helium flow prior to entering the pebble bed closely matches the designed inlet flow velocity of 0.1 m/s. As helium enters the pebble bed, the flow velocities of the helium gas increase rapidly. The maximum helium flow velocity is reached at approximately 0.5 d into the bed. In the inner region, the velocity is varied from about 0.2 m/s to 0.25 m/s. The cross-sectional averaged flow velocity increases about 2.5 times. Again, the velocity of helium flow reaches its maximum point at a position of 0.5 d before exiting the pebble bed. Subsequently, the flow velocity drops to around 0.1 m/s when leaving the bed. This variation can be mainly attributed the gradual decrease in the effective cross-sectional porosity of the flow channel, from 1 before entering and after leaving the pebble bed to approximately 0.3822~0.4791 inside the pebble bed. The decrease in the effective porosity in the flow channel results in a rapid increase in gas flow rate. The position at approximately 0.5 d to the outlet and inlet of the pebble bed indicates the lowest porosity value, maximizing the helium flow velocity (refer to Figure 13b for details). It has been observed that the wall effect causes a change in the porosity of the pebble bed, resulting in the pebble bed with four periodic boundaries having the smallest porosity. Therefore, its flow velocity is larger than that of the other two pebble beds, as shown by the average flow velocity in the central region of the pebble bed in Figure 13a.

In addition, the localized velocity distribution of helium flow within the pebble bed was also analyzed. Figure 14a–c illustrate the streamline inside the three pebble beds with different boundaries. It is observable that the helium flow quickens upon entering the pebble bed and decelerates upon leaving, ultimately returning to its initial state. Furthermore, the cut-plane method was utilized to calculate the average flow velocity and corresponding porosity of the pebble bed in the x and y directions parallel to the flow. The resulting data are presented in Figure 15, illustrating the velocity distribution of helium flow in a pebble bed with two fixed walls and two periodic boundaries in the x - and y -axis directions. Due to the fixed wall on the x -axis, the porosity along the x -axis varies significantly, leading to a perturbation of the average flow velocity within the pebble bed. As the pebble bed's fixed wall is non-slip, the velocity near it is 0. As the distance from the wall increases, the helium velocity increases rapidly, reaching a maximum value within a

range of less than $0.2d$ from the wall. As the distance from the fixed wall further increases, the average flow velocity of helium fluid varies in correspondence with the porosity variation. This is explained by the fact that larger porosities parallel to the direction of flow offer less resistance to helium, resulting in a similar flow velocity perturbation law to that of the porosity perpendicular to the wall direction, which allows a portion of the bypassed helium flow to exist in the area near the fixed wall.

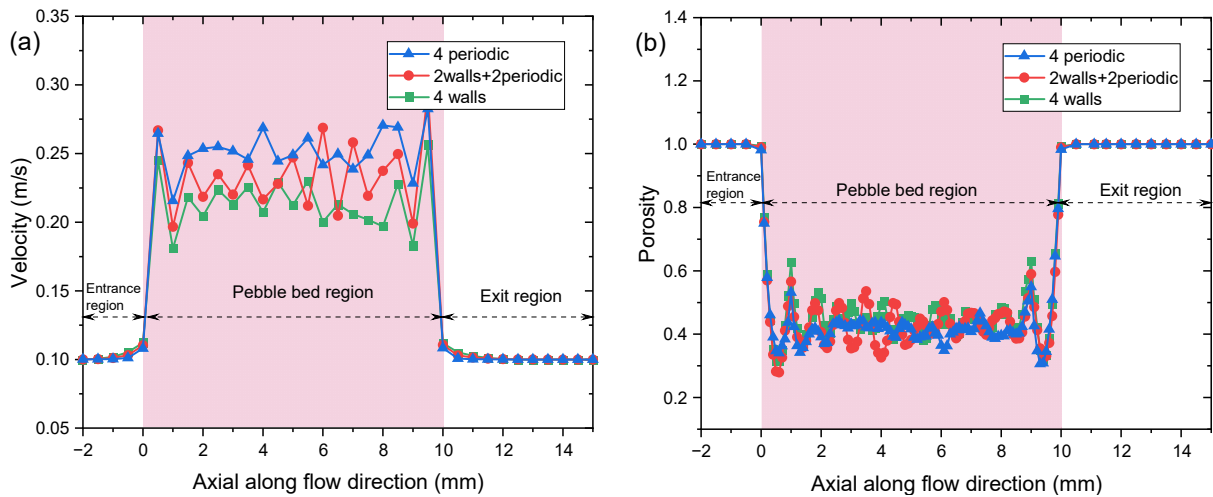


Figure 13. Velocity (a) and porosity distribution (b) along the flow direction in pebble beds with different boundary walls.

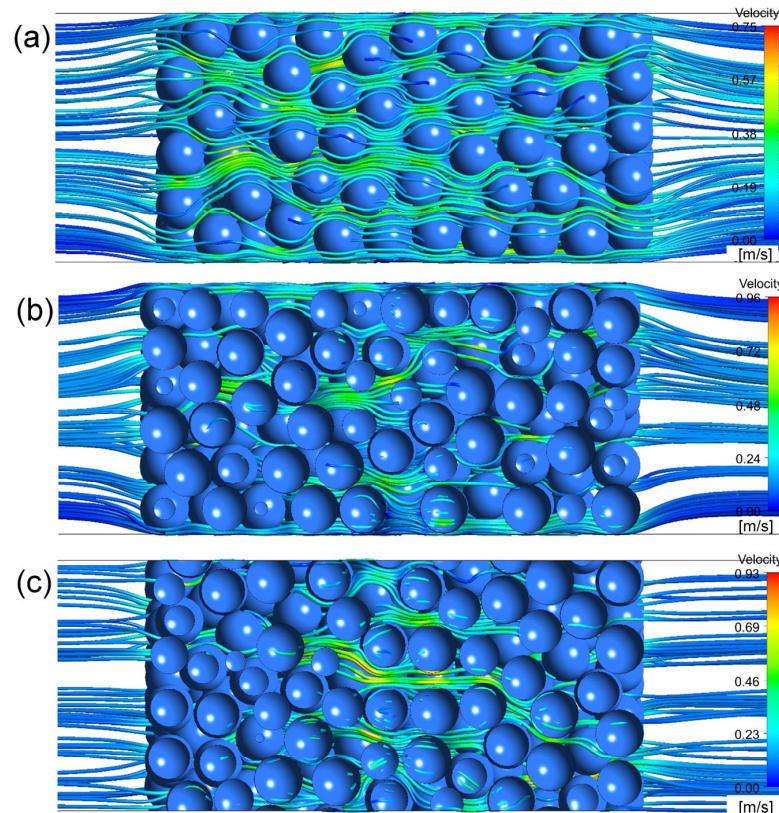


Figure 14. Streamline of purge gas in pebble beds with different boundary walls: (a) 4 fixed walls, (b) 2 fixed walls and 2 periodic boundaries, and (c) 4 periodic boundaries.

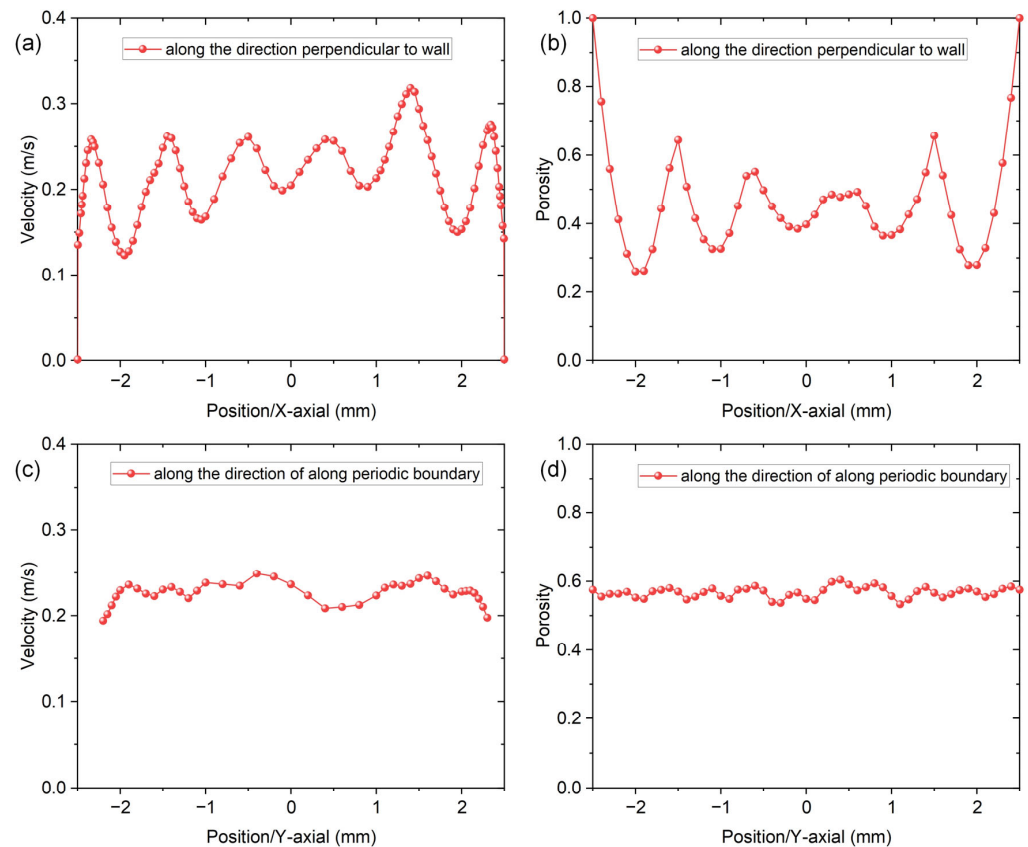


Figure 15. Velocity and porosity distribution along x - and y -axes in pebble bed with 2 fixed walls and 2 periodic boundaries: (a,c) average velocity distribution, (b,d) porosity distribution.

4. Conclusions

The numerical investigation of the flow behaviors of helium, used for purging tritium, inside pebble beds with three different wall boundary conditions was conducted using the combined DEM and CFD method. The conclusions may be summarized in the following points:

- The fixed wall significantly affected the packing structure of the pebble bed, resulting in the regular packing of some pebbles adjacent to the wall. Notably, the porosity of the pebble bed adjacent to the fixed wall displayed a remarkable oscillation.
- The helium pressure decreases uniformly and linearly in the pebble bed along the flow direction. The pressure drop gradient of helium within the pebble bed gradually increases with an increase in the packing factor of the pebble bed.
- The velocity of helium flow rapidly increases after entering the pebble bed due to the reduced cross-sectional area of the flow channel. The trend of the helium gas varies inversely to changes in porosity. In contrast, perpendicular to the direction of gas flow, the cut-plane averaged flow velocity of helium shows a similar variation to porosity.

Author Contributions: Conceptualization, B.G., H.C., B.Z., J.Y., L.W., L.Z., Y.F. and X.W.; Methodology, B.G., H.C., B.Z. and Y.F.; Software, B.G. and H.C.; Validation, B.G.; Data curation, B.G. and H.C.; Visualization, B.G.; Formal analysis, B.G.; Investigation, B.G. and H.C.; Writing—original draft preparation, B.G.; Writing—review and editing, B.G., H.C., B.Z., J.Y., L.W., L.Z., Y.F. and X.W.; Supervision, Y.F. and X.W.; Project administration, L.Z. and X.W. All authors have read and agreed to the published version of the manuscript.

Funding: This research was funded by the Chinese National Special Project for Magnetic Confined Nuclear Fusion Energy (Grant No. 2022YFE03210100 and 2017YFE0300602), the Natural Science

Foundation of Sichuan, China, (Grant No. 2022NSFSC1216), The Innovation Program of SWIP (Grant No. 202301XWCX004), and The National Natural Science Foundation of China (Grant No. 52276052).

Institutional Review Board Statement: Not applicable.

Informed Consent Statement: Not applicable.

Data Availability Statement: The data presented in this study are available on request from the corresponding author. The data are not publicly available due to privacy.

Acknowledgments: The authors acknowledge the support by HPC Platform, Southwestern Institute of Physics.

Conflicts of Interest: The authors declare no conflicts of interest.

Nomenclature

d	Diameter of pebbles
E	Young's modulus
e	Restitution coefficient
F_n	Normal contact force between two touched pebbles
F_t	Tangential contact force between two touched pebbles
G	Shear modulus
g	Gravitational acceleration
H	Length of pebble beds
I_i	The motion of inertia of pebble i
k_n	The elastic constant of normal contact (also known as normal stiffness)
k_t	The elastic constant of tangential contact (also known as tangential stiffness)
m_i	The mass of pebble i
N	Total pebble number
N_{cn}	Contact pebble number
P_{out}	Outlet relative pressure
P_{amb}	Ambient base pressure
ΔP	Pressure loss
R	The radius of a pebble
r_{ij}	The vector pointing from the pebble i to pebble j
U	Velocity of fluid
V_i	The velocity of the translational of pebble i
v_{in}	Inlet flow velocity
ω_i	The velocity of rotational movement of pebble i
Greek symbols	
ρ	Density of fluid
ρ_p	Density of pebbles
ε	Porosity
γ	Packing factor
ν	Poisson ratio
μ	The dynamic viscosity of the fluid
μ_{fri}	Friction coefficient between pebbles
η_n	The normal viscoelastic damping coefficient
$\delta_{n_{ij}}$	The overlap of two normal contact pebbles
$v_{n_{ij}}$	The normal relative velocity of two pebbles
η_t	The tangential viscoelastic damping coefficient
$\delta_{t_{ij}}$	The tangential relative displacement vector of two contact pebbles
$v_{t_{ij}}$	The tangential relative velocity of two pebbles
Abbreviation	
CFD	Computational Fluid Dynamics
DEM	Discrete Element Method
HCCB	Helium-Cooled Ceramic Breeder
TBM	Test Blanket Module
TES	Tritium Extraction System

References

1. Rubel, M. Fusion Neutrons: Tritium Breeding and Impact on Wall Materials and Components of Diagnostic Systems. *J. Fusion Energy* **2018**, *38*, 315–329. [[CrossRef](#)]
2. Wang, X.Y.; Feng, K.M.; Chen, Y.J.; Zhang, L.; Feng, Y.J.; Wu, X.H.; Liao, H.B.; Ye, X.F.; Zhao, F.C.; Cao, Q.X.; et al. Current design and R&D progress of the Chinese helium cooled ceramic breeder test blanket system. *Nucl. Fusion* **2019**, *59*, 076019.
3. Feng, Y.; Gong, B.; Cheng, H.; Luo, X.; Wang, L.; Wang, X. Effects of bed dimension, friction coefficient and pebble size distribution on the packing structures of the pebble bed for solid tritium breeder blanket. *Fusion Eng. Des.* **2021**, *163*, 112156. [[CrossRef](#)]
4. Gong, B.; Cheng, H.; Feng, Y.; Luo, X.; Wang, L.; Wang, X. Effect of Pebble Size Distribution and Wall Effect on Inner Packing Structure and Contact Force Distribution in Tritium Breeder Pebble Bed. *Energies* **2021**, *14*, 449. [[CrossRef](#)]
5. Chen, L.; Chen, Y.; Huang, K.; Liu, S. Investigation of the packing structure of pebble beds by DEM for CFETR WCCB. *J. Nucl. Sci. Technol.* **2016**, *53*, 803–808. [[CrossRef](#)]
6. Lei, M.; Song, Y.; Ye, M.; Lu, K.; Pei, K.; Xu, K.; Xu, S. Conceptual Design of a Helium-Cooled Ceramic Breeder Blanket for CFETR. *Fusion Sci. Technol.* **2015**, *68*, 772–779. [[CrossRef](#)]
7. Abdou, M.; Riva, M.; Ying, A.; Day, C.; Loarte, A.; Baylor, L.R.; Humrickhouse, P.; Fuerst, T.F.; Cho, S. Physics and technology considerations for the deuterium–tritium fuel cycle and conditions for tritium fuel self sufficiency. *Nucl. Fusion* **2020**, *61*, 013001. [[CrossRef](#)]
8. Wang, X.; Ran, G.; Wang, H.; Xiao, C.; Zhang, G.; Chen, C. Current Progress of Tritium Fuel Cycle Technology for CFETR. *J. Fusion Energy* **2018**, *38*, 125–137. [[CrossRef](#)]
9. Abou-Sena, A.; Arbeiter, F.; Boccaccini, L.V.; Rey, J.; Schlindwein, G. Experimental study and analysis of the purge gas pressure drop across the pebble beds for the fusion HCPB blanket. *Fusion Eng. Des.* **2013**, *88*, 243–247. [[CrossRef](#)]
10. Abou-Sena, A.; Arbeiter, F.; Boccaccini, L.V.; Schlindwein, G. Measurements of the purge helium pressure drop across pebble beds packed with lithium orthosilicate and glass pebbles. *Fusion Eng. Des.* **2014**, *89*, 1459–1463. [[CrossRef](#)]
11. Wang, M.; Liu, D.; Xiang, Y.; Cui, S.; Su, G.; Qiu, S.; Tian, W. Experimental study of the helium flow characteristics in pebble-bed under the condition of CFETR's blanket module. *Progress Nucl. Energy* **2017**, *100*, 283–291. [[CrossRef](#)]
12. Liu, D.; Tian, W.; Su, G.H.; Qiu, S. Experimental study on helium pressure drop across randomly packed bed for fusion blanket. *Fusion Eng. Des.* **2017**, *122*, 47–51. [[CrossRef](#)]
13. Panchal, M.; Saraswat, A.; Chaudhuri, P. Experimental measurements of gas pressure drop of packed pebble beds. *Fusion Eng. Des.* **2020**, *160*, 111836. [[CrossRef](#)]
14. Chen, Y.; Chen, L.; Liu, S.; Luo, G. Flow characteristics analysis of purge gas in unitary pebble beds by CFD simulation coupled with DEM geometry model for fusion blanket. *Fusion Eng. Des.* **2017**, *114*, 84–90. [[CrossRef](#)]
15. Wu, Z.; Wu, Y.; Tang, S.; Liu, D.; Qiu, S.; Su, G.H.; Tian, W. DEM-CFD simulation of helium flow characteristics in randomly packed bed for fusion reactors. *Progress Nucl. Energy* **2018**, *109*, 29–37. [[CrossRef](#)]
16. Cheng, H.; Fan, L.; Zhou, B.; Gong, B.; Wang, X.; Feng, Y. Numerical modeling on helium flow characteristics in tritium breeder pebble bed. *Nucl. Fusion Plasma Phys.* **2021**, *41*, 610–616.
17. Zhou, B.; Feng, Y.; Wang, X.; Wu, X. Thermal analysis for gas containing tritium in tritium breeding blanket of the test blanket module. *Nucl. Fusion Plasma Phys.* **2018**, *38*, 339–343.
18. Choi, D.; Park, S.; Han, J.; Ahn, M.-Y.; Lee, Y.; Park, Y.-H.; Cho, S.; Sohn, D. A DEM-CFD study of the effects of size distributions and packing fractions of pebbles on purge gas flow through pebble beds. *Fusion Eng. Des.* **2019**, *143*, 24–34. [[CrossRef](#)]
19. Lee, Y.; Choi, D.; Hwang, S.-P.; Ahn, M.-Y.; Park, Y.-H.; Cho, S.; Sohn, D. Numerical investigation of purge gas flow through binary-sized pebble beds using discrete element method and computational fluid dynamics. *Fusion Eng. Des.* **2020**, *158*, 111704. [[CrossRef](#)]
20. Lei, M.; Liu, S.; Wu, Q.; Xu, S.; Li, B.; Li, C. Research on purge gas flow characteristics in different pebble bed structures for fusion blanket. *Progress Nucl. Energy* **2023**, *155*, 104488. [[CrossRef](#)]
21. Zhang, H.; Li, Z.; Guo, H.; Ye, M.; Huang, H. DEM-CFD simulation of purge gas flow in a solid breeder pebble bed. *Fusion Eng. Des.* **2016**, *113*, 288–292. [[CrossRef](#)]
22. Sedani, C.; Panchal, M.; Chaudhuri, P. Simulation and experimental analysis of purge gas flow characteristic for pebble bed. *Fusion Eng. Des.* **2021**, *172*, 112778. [[CrossRef](#)]
23. Desu, R.K.; Moorthy, A.; Annabattula, R.K. DEM simulation of packing mono-sized pebbles into prismatic containers through different filling strategies. *Fusion Eng. Des.* **2018**, *127*, 259–266. [[CrossRef](#)]
24. Gui, N.; Jiang, S.; Yang, X.; Tu, J. A review of recent study on the characteristics and applications of pebble flows in nuclear engineering. *Exp. Comput. Multiph. Flow* **2022**, *4*, 339–349. [[CrossRef](#)]
25. Jaggannagari, S.R.; Desu, R.K.; Reimann, J.; Gan, Y.; Moscardini, M.; Annabattula, R.K. DEM simulations of vibrated sphere packings in slender prismatic containers. *Powder Technol.* **2021**, *393*, 31–59. [[CrossRef](#)]
26. Kim, D.-O.; Hwang, S.-P.; Sohn, D. DEM study of packing and connectivity of binary-sized pebbles according to their size and mixing ratios under vibration conditions. *Fusion Eng. Des.* **2021**, *168*, 112648. [[CrossRef](#)]
27. Wang, S.; Wang, S.; Chen, H. Numerical influence analysis of the packing structure on ceramic breeder pebble beds. *Fusion Eng. Des.* **2019**, *140*, 41–47. [[CrossRef](#)]
28. Atmakidis, T.; Kenig, E.Y. CFD-based analysis of the wall effect on the pressure drop in packed beds with moderate tube/particle diameter ratios in the laminar flow regime. *Chem. Eng. J.* **2009**, *155*, 404–410. [[CrossRef](#)]

29. Guo, Z.; Sun, Z.; Zhang, N.; Ding, M. Influence of confining wall on pressure drop and particle-to-fluid heat transfer in packed beds with small D/d ratios under high Reynolds number. *Chem. Eng. Sci.* **2019**, *209*, 115200. [[CrossRef](#)]
30. van der Merwe, W.J.S.; du Toit, C.G.; Kruger, J.H. Influence of the packing structure on the flow through packed beds with small cylinder diameter to particle diameter ratios. *Nucl. Eng. Des.* **2020**, *365*, 110700. [[CrossRef](#)]
31. Zhang, B.; Wang, B.; Yan, S.; Bai, Z.; Hu, Z.; Lu, Z. CFD-DEM coupling simulation of fixed bed reactor with small diameter ratio. *J. Dispers. Sci. Technol.* **2020**, *42*, 1747–1755. [[CrossRef](#)]
32. Kloss, C.; Goniva, C.; Hager, A.; Amberger, S.; Pirker, S. Models, algorithms and validation for opensource DEM and CFD-DEM. *Progress Comput. Fluid Dyn. Int. J.* **2012**, *12*, 140–152. [[CrossRef](#)]
33. *LIGGGHTS(R)-PUBLIC Documentation*, Version 3.X; DCS Computing GmbH: Linz, Austria, 2024.
34. Cundall, P.A.; Strack, O.D.L. A discrete numerical model for granular assemblies. *Géotechnique* **1979**, *29*, 47–65. [[CrossRef](#)]
35. Wang, J.; Lei, M.Z.; Xu, S.L.; Yang, H.; Zhao, P.H.; Xu, K.; Song, Y.T. DEM simulation of mechanical behavior in one-dimensional compression of crushable ceramic pebble bed. *Fusion Eng. Des.* **2021**, *168*, 112606. [[CrossRef](#)]
36. Pichler, M.; Haddadi, B.; Jordan, C.; Norouzi, H.; Harasek, M. Effect of particle contact point treatment on the CFD simulation of the heat transfer in packed beds. *Chem. Eng. Res. Des.* **2021**, *165*, 242–253. [[CrossRef](#)]
37. Calis, H.P.A.; Nijenhuis, J.; Paikert, B.C.; Dautzenberg, F.M.; van den Bleek, C.M. CFD modelling and experimental validation of pressure drop and flow profile in a novel structured catalytic reactor packing. *Chem. Eng. Sci.* **2001**, *56*, 1713–1720. [[CrossRef](#)]
38. *Ansys CFX-Solver Theory Guide*; 2021R1; Ansys Inc.: Canonsburg, PA, USA, 2021.
39. Klerk, A.D. Voidage variation in packed beds at small column to particle diameter ratio. *AIChE J.* **2003**, *49*, 2022–2029. [[CrossRef](#)]
40. Reimann, J.; Vicente, J.; Ferrero, C.; Rack, A.; Gan, Y. 3d tomography analysis of the packing structure of spherical particles in slender prismatic containers. *Int. J. Mater. Res.* **2020**, *111*, 65–77. [[CrossRef](#)]

Disclaimer/Publisher’s Note: The statements, opinions and data contained in all publications are solely those of the individual author(s) and contributor(s) and not of MDPI and/or the editor(s). MDPI and/or the editor(s) disclaim responsibility for any injury to people or property resulting from any ideas, methods, instructions or products referred to in the content.